Fibroblast Network in Rabbit Sinoatrial Node: Structural and Functional Identification of Homogeneous and Heterogeneous Cell Coupling

Patrizia Camelliti, Colin R. Green, Ian LeGrice and Peter Kohl

Circ. Res. 2004;94;828-835; originally published online Feb 19, 2004;
DOI: 10.1161/01.RES.0000122382.19400.14
Circulation Research is published by the American Heart Association. 7272 Greenville Avenue, Dallas, TX 72514
 Print ISSN: 0009-7330. Online ISSN: 1524-4571

Fibroblast Network in Rabbit Sinoatrial Node

Structural and Functional Identification of Homogeneous and Heterogeneous Cell Coupling

Patrizia Camelliti, Colin R. Green, Ian LeGrice, Peter Kohl

Abstract—Cardiomyocytes form a conducting network that is assumed to be electrically isolated from nonmyocytes in vivo. In cell culture, however, cardiac fibroblasts can contribute to the spread of excitation via functional gap junctions with cardiomyocytes. To assess the ability of fibroblasts to form gap junctions in vivo, we combine in situ detection of connexins in rabbit sinoatrial node (a tissue that is particularly rich in fibroblasts) with identification of myocytes and fibroblasts using immunohistochemical labeling and confocal microscopy. We distinguish two spatially distinct fibroblast populations expressing different connexins: fibroblasts surrounded by other fibroblasts preferentially express connexin40, whereas fibroblasts that are intermingled with myocytes largely express connexin45. Functionality of homogeneous and heterogeneous cell coupling was investigated by dye transfer in sinoatrial node tissue explants. These studies reveal spread of Lucifer yellow, predominantly along extended threads of interconnected fibroblasts (probably via connexin40), and occasionally between neighboring fibroblasts and myocytes (probably via connexin45). Our findings show that cardiac fibroblasts form a coupled network of cells, which may be functionally linked to myocytes in rabbit SAN. **(*Circ Res*. 2004;94:828-835.)**

Key Words: heart ■ connective tissue ■ pacemaker ■ gap junction ■ in vivo

Cardiomyocytes in vivo are thought to form a conducting network that is electrically isolated from nonmyocytes. However, cocultured neonatal rat cardiac myocytes and fibroblasts readily form functional gap junctions.[1,2] In vitro, this heterogeneous electrical interaction is sufficient to synchronize the contractile activity of distant cardiomyocytes, interconnected by one or more fibroblasts.[3] Whether similar behavior may occur in vivo is a subject of considerable debate.[4]

Earlier electrophysiological studies with double-barreled floating microelectrodes provided circumstantial evidence for capacitative and electrotonic myocyte-fibroblast coupling in spontaneously beating rat right atrium.[5] In contrast, transmission electron microscopy of serial cross sections of rabbit right-atrial tissue yielded only "one tiny gap junction–like structure" between a myocyte and a fibroblast in a tissue volume assumed to contain 10^4 homogeneous myocyte-myocyte connections.[6] Recent confocal microscopy of living rabbit sinoatrial node (SAN), performed using the vital dye CellTracker (CMFDA, Molecular Probes), demonstrated an abundance of myocyte-fibroblast membrane appositions in rabbit SAN.[7] Whether these areas contain dispersed gap junctional channels that provide heterogeneous coupling without forming an electron-dense substrate for electron-microscopic recognition (as reported in pig coronary artery)[8] is unknown.[9]

The general distribution of gap junction protein in rabbit SAN has been studied using immunohistochemical techniques. Both connexin45 (Cx45) and connexin40 (Cx40) have been found,[10–13] but coupled cell types were not identified. Data on fibroblast gap junction coupling has mainly been obtained in other organs (eg, skin, kidney, and cornea) or in cardiac cell cultures,[2] where cells are predominantly coupled by connexin43 (Cx43).

In this study, we use confocal laser-scanning microscopy and immunohistochemical techniques to combine localization of the three main cardiac connexins (Cx40/Cx43/Cx45) with positive cell type identification of myocytes and fibroblasts, as well as Lucifer yellow (LY) dye spread, to investigate homogeneous and heterogeneous cell coupling in native rabbit SAN tissue.

Materials and Methods

General Preparation

Cardiac tissue was obtained from New Zealand White rabbits (Animal Resources Unit, University of Auckland, New Zealand), killed by cervical dislocation (rabbits $\leq$1 kg, n=8) or anesthetized terminally by intraperitoneal injection of heparinized (200 U$\times$kg^{-1}) pentobarbitone-sodium (65 mg$\times$kg^{-1}; rabbits $>$1 kg, n=12). The chest was opened and the heart swiftly removed and washed by coronary perfusion with oxygenated Tyrode solution containing

Original received August 28, 2003; resubmission received November 11, 2003; revised resubmission received February 4, 2004; accepted February 5, 2004.

From the University Laboratory of Physiology (P.C., P.K.), Oxford, UK; Departments of Anatomy with Radiology (C.R.G.) and of Physiology (I.L.), University of Auckland, Auckland, New Zealand.

Correspondence to Peter Kohl, University Laboratory of Physiology, Oxford, OX1 3PT, UK. E-mail peter.kohl@physiol.ox.ac.uk

Circulation Research **is available at http://www.circresaha.org** **DOI: 10.1161/01.RES.0000122382.19400.14**

(in mmol/L) 140 NaCl, 5.4 KCl, 1.0 $MgCl_2$, 8.0 HEPES, 1.8 $CaCl_2$, and 10 Glucose; pH 7.4.

Structural Studies

SAN Tissue Specimen

The SAN was dissected from the right atrium and placed into a drop of Tissue-Tek (Miles Inc) on top of a silanized glass slide. One to four no.1 cover slips were positioned at either end of the slide (depending on the thickness of the node), and a second silanized glass slide was placed over the top, flattening the node between the slides to a thickness of 170 to 680 μm. This preparation was quickly plunge-frozen in liquid nitrogen. The procedure from sacrifice to tissue freezing took about 10 minutes.

Slides were separated, and the frozen embedded node placed onto a precooled Tissue-Tek coated cryotome chuck (horizontally, endocardium up). Care was taken to avoid thawing before the chuck was further cooled in liquid nitrogen. Using a cryotome, 40 to 60 μm of the endocardial surface was removed to expose nodal cardiomyocytes beneath the outer connective tissue layer. Then 16 μm cryosections were cut in the plane of the SAN, collected on SuperFrost slides (Menzel-Glaser, Germany) and stored at −80°C.

For positive control experiments on anti-connexin antibody functionality, ventricular tissue from 3 rabbits was collected and handled as described above.

Antibodies

For Cx40, we used guinea pig polyclonal antibodies, raised against an oligopeptide matching the cDNA-sequence of the carboxy-terminus (amino acids 256 to 270, *V15K/GP318*),[14,15] and for Cx45, a guinea pig polyclonal antibody raised against the cytoplasmic carboxy-terminal region (amino acids 354 to 367, *Q14E/GP42*).[11,15] Antibodies were kindly provided by Drs S.R. Coppen, N. Severs (both of Imperial College London, England), and R.G. Gourdie (Medical University of South Carolina, Charleston, SC). For Cx43, a mouse monoclonal antibody, raised against a short peptide sequence (amino acids 131 to 142) of the protein cytoplasmic loop, was kindly provided by Dr D. Becker (University College London, England).[16] Myocyte M-lines were labeled using mouse anti-myomesin antibodies (clone B4)[17] kindly supplied by Dr H.M. Eppenberger (ETH Zürich, Switzerland), and fibroblasts were identified using mouse monoclonal anti-vimentin antibodies (clone V9 Sigma Aldrich)[18,19] that label intermediate filaments, which are particularly abundant in fibroblasts.

Immunolabeling

Tissue sections were fixed in cold acetone (10 minutes), washed with PBS, and blocked for 1 hour at room temperature (RT) in 10% serum/0.3% bovine serum albumin (BSA)/0.1% TritonX-100 in PBS.

For single labeling, slides were incubated overnight (O/N) at 4°C with primary antibodies (diluted in PBS/0.3% BSA/0.1% TritonX-100) and with CY3- (543 nm excitation, 555 to 700 nm emission detected; Jackson Immuno Research Laboratories Inc), Alexa488- (488 nm excitation, 500 to 535 nm emission detected; Molecular Probes Inc) or FITC- (488 nm excitation, 500 to 535 nm emission detected; DAKO Corp) conjugated secondary antibodies (2 hour RT). A washing step in PBS was performed between antibody incubations.

For double labeling of connexins and cell types, sections were incubated with anti-connexin antibodies (O/N 4°C; anti-Cx45 1:200, anti-Cx40 1:500) and CY3-conjugated secondary antibodies (1:500, 2 hour RT), and subsequently with either anti-vimentin (O/N 4°C; 1:1000) and secondary rabbit anti-mouse FITC (1:100, 2 hour RT), or anti-myomesin (1:100, O/N 4°C) and secondary goat anti-mouse Alexa488 (1:500, 2 hour RT).

For triple antibody incubation, samples were exposed to anti-Cx40/anti-Cx45 (O/N 4°C) and the secondary CY3-conjugated antibody (1:500, 2 hour RT), then mouse anti-myomesin (1:100, O/N 4°C) and secondary goat anti-mouse Alexa488 (1:500, 2 hour RT), and finally mouse anti-vimentin (1:1000, O/N 4°C) and secondary rabbit anti-mouse FITC (1:100, 2 hour RT).

Control experiments involved omission of primary antibodies and incubation with inappropriate secondary antibodies to exclude cross-reactivity. Positive control experiments on ventricular tissue confirmed antibody functionality. All sections were mounted in Citi-Fluor antifade medium (Agar Scientific, UK).

Confocal Microscopy

Immunolabeled sections were examined with a Leica TCS-SP2 confocal laser-scanning microscope. Single optical slices or z-series were recorded. Images were combined to localize gap junctions with respect to cell types. Myocytes and fibroblasts were identified based on cell morphology and characteristic labeling patterns of myomesin (for myocyte M-lines, revealing typical cross striation) and vimentin (for fibroblast intermediate filaments, revealing brightly labeled solid cells and their processes, see Figure 1).

CellTracker Dye Loading

CellTracker was applied to freshly isolated SAN preparations in cardioplegic solution (modified Tyrode containing 20 mmol/L KCl) at a concentration of 5 $\mu g \times mL^{-1}$. Nodes were left O/N (4°C), washed in cardioplegic solution (1 hour), and fixed using fresh 4% paraformaldehyde in PBS (RT). CellTracker diffuses freely through the cell membrane and, once inside, undergoes a glutathione s-transferase–mediated reaction to form a membrane-impermeant glutathione-fluorescent dye adduct. Fixed nodes were mounted in CitiFluor and viewed with a Leica TCS-4D confocal laser-scanning microscope, using 488 nm excitation and an FITC bandpass emission filter.

Quantification of Connexin Immunolabeling

Optical slice stacks showing Cx40 or Cx45 immunolabeling were obtained from the SAN of 5 and 6 different animals, respectively. For a direct comparison of Cx40/Cx45 expression levels in different cell types, images containing both fibroblast-rich (F) and myocyte/fibroblast-intermingled (MF) areas were examined (Cx40 n=11; Cx45 n=14). Images were quantitatively analyzed using ImageJ-1.29 (http://rsb.info.nih.gov/ij/). In each stack, one or more F and MF area(s) each were identified and defined as "regions of interest." Projections showing Cx40 or Cx45 immunolabeling only were produced from each stack, and fluorescent spots were counted in the respective regions of interest. Using a threshold-value algorithm, only spots of sufficiently high intensity were considered. The total area occupied by connexin immunoreactivity in each region was also analyzed. Connexin density was expressed as (1) the cumulative number of gap junctions per tissue volume (calculated from stack-depth and dimensions of the region of interest), and (2) the area occupied by connexin fluorescence relative to the total scanned tissue area. Connexin densities in neighboring F versus MF areas were compared using the nonparametric paired Wilcoxon test (GraphPad Prism). Data are presented as mean±SEM (Table).

To establish how common heterogeneous myocyte-fibroblast coupling by Cx45 is in MF areas, the number of Cx45 plaques between myocytes and fibroblasts was counted in 200 optical sections, obtained in 33 SAN locations from 8 different animals. Only spots that were clearly identified as being located exactly at the point of contact of two heterogeneous cells were included (in particular, connexin labeling at contact sites of potentially more than two cells was disregarded). Heterogeneous Cx45 density was then compared with total Cx45 density in the same tissue regions.

Functional Studies

Scrape-Loading of Lucifer Yellow

Hearts, excised from New Zealand White rabbits (≤1 kg, n=12), were washed by Langendorff perfusion (oxygenated Tyrode solution, 37°C, 5 to 10 minutes). The SAN region, including crista terminalis (CT), orifices of the opened venae cavae, and part of the interatrial septum, were dissected out and pinned into a sylgard-based Petri dish (endocardium up). Scrape-loading was used to introduce LY (2.5 $mg \times mL^{-1}$) and Texas red dextran (0.5 $mg \times mL^{-1}$).[20–22] In brief, cells that are nonterminally damaged by scraping with a sharp instrument take up the dyes (intact cell

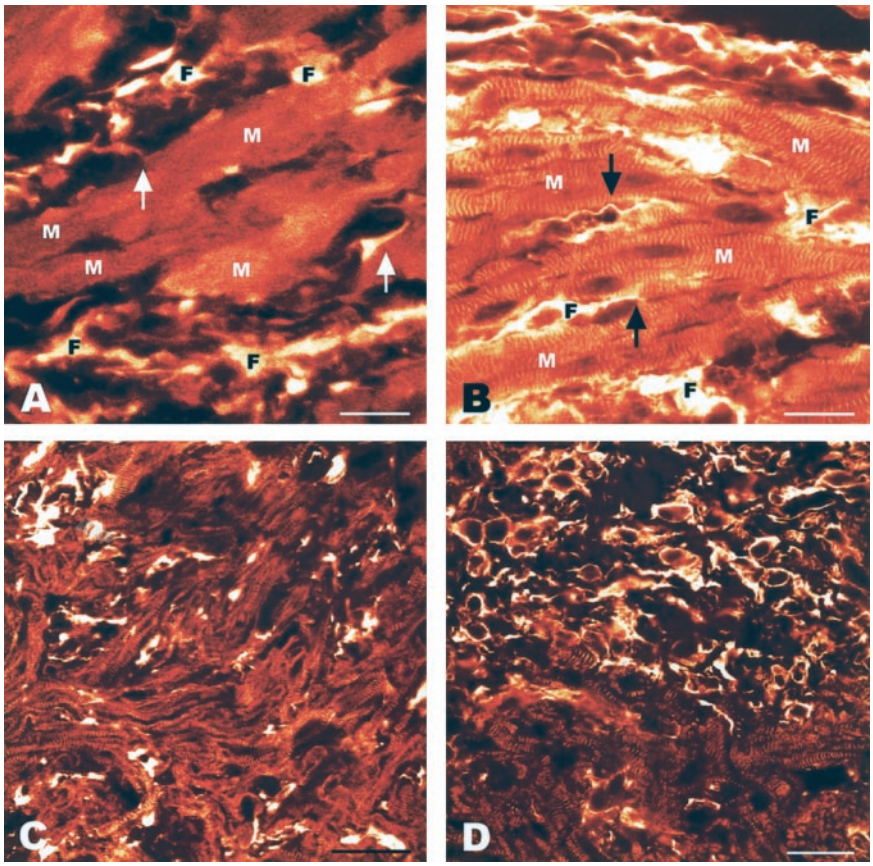

Figure 1. Fibroblast-myocyte interrelation in rabbit sinoatrial node (SAN). A, Confocal laser-scanning image of freshly isolated SAN after CellTracker diffusion loading. Groups of SAN myocytes (M; central, large, more uniformly labeled patches) are intermingled with fibroblasts (F; smaller, more brightly stained cells) with numerous fine processes extending between and alongside myocytes (arrows). B, Confocal optical section of peripheral SAN, labeled with anti-vimentin (for fibroblast intermediate filaments, revealing brightly labeled "solid" cells and their processes; F) and anti-myomesin antibodies (for myocyte M-lines, revealing typical cross striations; M). Numerous fibroblast processes extend between myocytes and contact them (arrows). C and D, Confocal optical sections of central SAN, showing tissue where myocytes (striated cells) and fibroblasts (more uniformly, brightly labeled cells) intermingle (C), compared with areas dominated by fibroblasts (top two thirds of D). Scale bars=20 μm.

membranes are impermeable to both dyes). Texas red dextran is too large to pass through gap junctions and remains trapped in primary loaded cells (marking scrape-loaded cells). In contrast, LY is able to spread to neighboring cells via gap junctions. Cells located away from the loading site that contain LY (but no Texas red dextran) are understood to be coupled by gap junctions to primary scrape-loaded cells.

In this study, a droplet of PBS, containing LY and Texas red dextran, was placed onto the auricular CT, and several fine holes (100 μm insect dissection pins) were made transmurally to allow dye penetration (for 2 minutes). The preparation was then washed with Tyrode solution, with the dish angled so that fresh solution was supplied from the SAN side and drained over CT and auricular muscle. After a further 2 to 5 minutes, the tissue was fixed in fresh 4% paraformaldehyde in PBS (1 hour RT) and washed for several hours (PBS). The epicardial CT was partially trimmed and the preparation mounted between two long coverslips, spaced at 170 μm, for viewing from either side. Control tissue was handled as above, but with omission of dyes, and revealed negligible autofluorescence with the exception of narrow but well-defined fibrous layers ($<$10 μm) at the endo- and epicardial surfaces.

Confocal Microscopy for Lucifer Yellow

Preparations were viewed with a Leica TCS-SP2 confocal laser-scanning microscope using 458 and 476 nm excitation and 489 to 600 nm emission for LY, and 543 nm excitation and 555 to 620 nm emission for Texas red dextran. LY becomes more readily visible at these excitation and emission wavelengths after fixation in paraformaldehyde.[23] Cells containing the gap junction impermeable Texas red dextran identified primary scrape-loaded cells; cells located away from the transmural loading site ($\geq$200 μm transversal to the direction of pin-holes), containing LY only, were regarded as having received the dye via gap junctions.

Experiments complied with UK Home Office regulations and had Animal Ethics Committee approval.

Results

Cell Type Identification

Myocyte/fibroblast spatial interrelation in the SAN was investigated using loading of living pacemaker tissue with CellTracker and immunohistochemical labeling of SAN cryosections using cell-type specific antibodies.

CellTracker labels the cytoplasm of living cells only. SAN fibroblasts, identified by their cell morphology (established from confocal optical slice series), become preferentially labeled, indicating greater membrane permeability over myocytes, or increased glutathione s-transferase activity. CellTracker allowed detection of even the finest fibroblast processes, reconfirming the presence of numerous membrane appositions between myocytes and fibroblasts in rabbit SAN (Figure 1A).

This is also observed using cell type–specific antibodies. Anti-vimentin labeled fibroblasts (Figure 1B), whose individual cytoarchitecture and topology matches that observed with CellTracker, whereas anti-myomesin allowed myocyte identification. More peripheral areas of the SAN show increasing alignment of sarcomeres and myocytes, and larger (atrial) muscle cells. The more central SAN, in contrast, is characterized by significantly smaller and less ordered myocytes with reduced myomesin density. Throughout the SAN, MF areas (where myocytes and fibroblasts intermingle; Figure 1C) were found adjacent to F areas (dominated by fibroblasts; Figure 1D).

Connexins and Cell Type Labeling

A crucial feature of these SAN preparations is the fact that sectioning occurred in the en face plane of the frozen tissue.

Connexin40 and Connexin45 Density in Rabbit Sinoatrial Node Tissue Areas of Intermingled Myocyte/Fibroblast Content Compared With Adjacent Fibroblast-Rich Areas Without Detectable Myocytes

	Connexin40						Connexin45					
	Spots$\times10^4\times mm^{-3}$			Area $\mu m^2\times mm^{-2}$			Spots$\times10^5\times mm^{-3}$			Area $\mu m^2\times mm^{-2}$		
n (Sample)	MF	F	F/MF	MF	F	F/MF	MF	F	F/M	MF	F	F/MF
1	31.3	96.5	3.1	79.5	417.3	5.2	198.8	3.1	0.01	2006.8	15.2	0.007
2	9.4	71.0	7.5	6.3	185.3	29.4	92.6	3.0	0.03	496.5	11.5	0.023
3	34.0	129.4	3.8	62.3	300.4	4.8	65.5	3.9	0.06	605.4	20.7	0.034
4	56.8	410.3	7.2	147.4	728.5	4.9	69	2.5	0.04	500.7	11.7	0.023
5	236.8	279.8	1.2	247.0	586.2	2.4	134	14.0	0.10	523.7	23.8	0.045
6	76.6	274.0	3.6	77.0	597.5	7.8	133.5	24.0	0.18	1411.6	120	0.085
7	68.0	258.3	3.8	55.2	491.7	8.9	89.6	4.4	0.05	615.5	17.4	0.028
8	16.7	97.7	5.8	12.0	354.1	29.5	250.4	17.6	0.07	676.6	8.9	0.013
9	6.4	29.7	4.6	22.4	173.0	7.7	348.2	24.9	0.07	1430	38.8	0.027
10	3.4	29.2	8.6	2.8	74.5	26.6	66.3	10.7	0.16	428.9	42.5	0.099
11	0.6	2.3	3.8	17.6	75.4	4.3	46.8	4.7	0.10	477.7	43.1	0.090
12							177.6	19.9	0.11	441.7	18.7	0.042
13							89.2	17.9	0.20	453	95.1	0.210
14							37.4	12.4	0.33	467.2	152.4	0.326
n		11			11			14			14	
Mean F/MF		4.83			12			0.11			0.075	
SE		0.67			3.3			0.023			0.024	
P		<0.001			<0.001			<0.0001			<0.0001	

Pairs of density values for connexin40 (left) and connexin45 (right) were obtained from adjacent tissue areas of the same slide that contained either a mix of myocytes and fibroblasts (MF), or preferentially fibroblasts (F). Densities in each slide were compared using a nonparametric paired Wilcoxon test and expressed as the ratio of F/MF. Number of gap junction–based density is expressed as spots per volume unit, whereas the area-based density is shown as area of connexin-related fluorescence divided by total area scanned.

Removal of the endocardial connective tissue layer exposed extended regions of continuous and undisturbed SAN pacemaker tissue for connexin mapping and cell-type identification.

Connexin40

Punctate Cx40 label was organized in clusters throughout the SAN. Double labeling for Cx40 and fibroblasts revealed that it is clearly present between SAN fibroblasts, whereas double labeling for Cx40 and myocytes revealed Cx40 predominantly in regions devoid of muscle-specific staining (not shown). Triple labeling for Cx40, myocytes, and fibroblasts, conducted over extensive SAN regions, confirmed that Cx40 is predominantly associated with fibroblasts. Figure 2A illustrates Cx40 labeling (green or yellow spots; color shift indicates colocalization of fluorochromes) in a fibroblast-rich area. There is very little Cx40 label associated with nodal myocytes seen in the upper and lower regions of this extended focus image taken from central SAN. A higher-magnification, single optical slice from a similar area, is shown in Figure 2B, illustrating Cx40 labeling between fibroblast processes.

Quantitative analysis established that the density of Cx40 gap junctions (number of gap junctions per tissue volume) is about five times greater in F areas than in MF regions ($152.6\pm39.9\times10^4$ spots$\times mm^{-3}$ versus $49.1\pm20.4\times10^4$ spots$\times mm^{-3}$, respectively; Table). This preferential localization of Cx40 is even more apparent when comparing the relative area occupied by Cx40 immunoreactivity, which is 12 times greater in F areas than elsewhere (362.2 ± 67.1 $\mu m^2\times mm^{-2}$ versus 66.3 ± 22.3 $\mu m^2\times mm^{-2}$, respectively; Table).

Connexin45

Patches of punctate Cx45 label were evident in regions with SAN myocytes, and wherever central SAN myocytes are in close proximity to fibroblast processes. In contrast, Cx45 was only rarely observed in fibroblast-rich areas devoid of myocytes.

Triple labeling identified the cell types associated with the Cx45 label. Cx45 label in the central SAN was located either between pairs of myocytes, between pairs of fibroblasts (Figure 2C, extended focus projection) or between heterogeneous myocyte-fibroblast pairs (Figures 2D and 3).

Figure 2D is a higher-magnification image of a single optical slice in the same region as Figure 2C, with at least two green spots (horizontal arrows) indicating Cx45 label between a nonmyocyte process and a myocyte. Very distinct points of Cx45 labeling were consistently detected exactly where heterogeneous cells make contact. Serial optical sections allowed us to locate the gap junctions at the end of fibroblast processes where they approach a myocyte surface. This is shown in Figure 3, where two fibroblast processes (arrows) that pass between myocytes have been followed through 1.5 μm. An identical optical slice series for the Cx45-specific marker revealed two gap junction plaques in

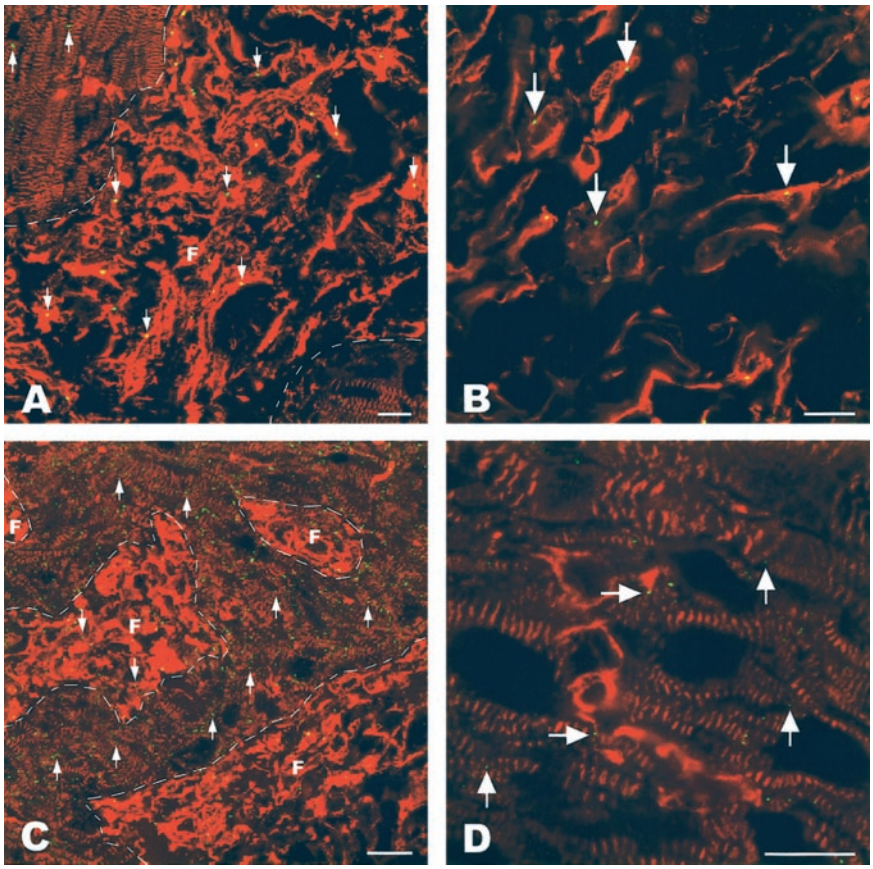

Figure 2. Labeling for Cx40 (top) or Cx45 (bottom), myomesin, and vimentin in rabbit SAN. A, Cx40 in a projection of 8 optical slices through 3.7 μm. Cx40 (green and yellow spots, arrows) is primarily located in fibroblast-rich tissue (F), demarcated by a dotted white line. B, Higher-magnification image (single optical slice) of a similar region as in A. Cx40-labeled gap junctions (arrows) are located among fibroblasts. C, Cx45 in a projection of 14 optical slices through 8 μm. In contrast to Cx40 in A, Cx45 (green and yellow spots, arrows) is predominantly located outside the fibroblast-rich regions. D, Higher-magnification image (single optical slice) of similar region as in C, showing Cx45 label between SAN myocytes (vertical arrows) and between fibroblasts and myocytes (horizontal arrows). Top horizontal arrow identifies a Cx45 spot between a fibroblast cell body and a myocyte underneath, whereas the lower horizontal arrow identifies a Cx45 spot between the process of a fibroblast cell located to the top left of the spot (as confirmed from neighboring optical sections) and a myocyte. Scale bars=10 μm.

the third optical slice (Figure 3C′), where one fibroblast process makes contact with a myocyte (left side of C in the myomesin-vimentin image series), while another one forms a contact with a process from a further fibroblast (right side of C in the myomesin-vimentin image series). In Figure 3C″, the Cx45 labeling seen in Figure 3C′ has been overlaid with the myomesin and vimentin labeling from Figure 3C to illustrate this.

Quantitative assessment confirms that the density of Cx45 gap junctions and their relative area are about one order of magnitude higher in MF regions compared with F areas (Table).

A total of 214 heterogeneous myocyte-fibroblast Cx45 gap junctions were identified in 33 SAN tissue preparations from 8 animals. The relative density (per area) of heterogeneous Cx45 contacts is 771.9±95.5 spots×mm^{-2}, compared with a total Cx45 density of 8348.7±1450.7 spots×mm^{-2} in MF regions, suggesting that just under 10% of Cx45 is located at points of heterogeneous cell contact.

Our direct comparison of Cx45 and Cx40 patterns in rabbit SAN therefore shows that they have spatially distinct locations: Cx40 is primarily present in F regions devoid of myocytes and Cx45 in areas where myocytes and fibroblasts intermingle. Our results also indicate that there are two distinct fibroblast populations in rabbit SAN, which express different connexins, depending on their histomorphological environment. Fibroblasts expressing Cx40 appear to be involved solely in homogeneous cell coupling, whereas fibroblasts expressing Cx45 would seem to be able to support both homogeneous and heterogeneous cell contacts.

Connexin43

As previously described,[12,24] we observed an abundance of well-organized Cx43 in the intercalated discs between atrial myocytes near the CT (Figure 4A). At the interface between the SAN and CT (Figure 4B), bundles of atrial muscle cells that express Cx43 protrude into the SAN. Cx43 in this area is not organized in intercalated discs, but arranged longitudinally along the atrial muscle fibers (resembling the Cx43 distribution of the developing heart[25] or infarct border zones).[26] There was no evidence for Cx43 in the more central SAN (neither in myocytes nor fibroblasts), as described previously.[27,28]

Functional Coupling of Cells in the SAN

Our immunohistochemical findings suggest that Cx40 may underlie fibroblast coupling, and Cx45 may support interaction between myocytes and fibroblasts in rabbit SAN. The presence of connexin immunolabeling alone does not confirm formation of functional gap junctions. To this end, we studied cell coupling by LY dye transfer into the SAN, following transmural scrape-loading of the auricular CT.

LY invades both peripheral and central SAN, revealing complex networks of dye-loaded fibroblasts and myocytes which, given their separation from the loading site, will have taken up the dye via gap junction–based cell-to-cell transfer. Figure 5 is a confocal optical slice z-series illustrating a pathway of LY from the CT scrape site (top right of images) that gives rise to preferential staining of a strand of fibroblasts and, deeper in the tissue (seen in subsequent optical slices),

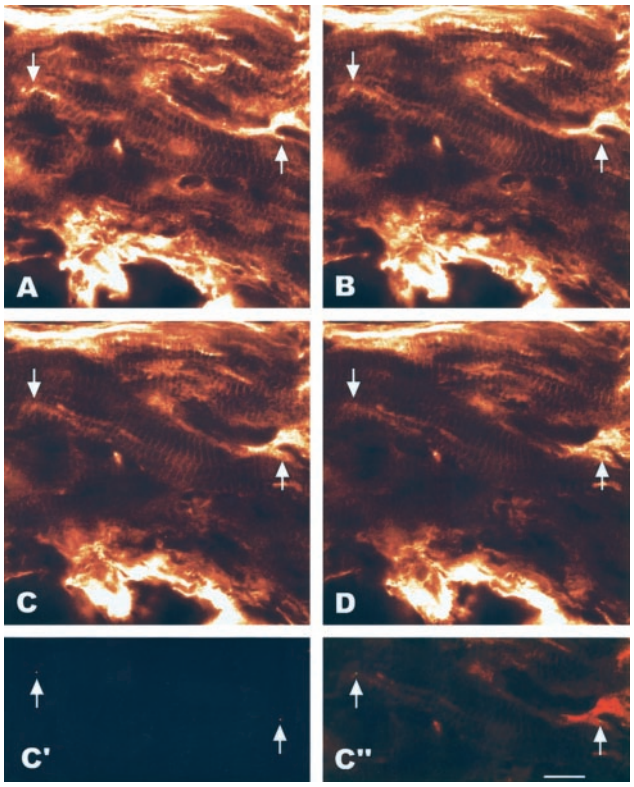

Figure 3. Labeling for Cx45, vimentin, and myomesin in rabbit SAN. A through D, Confocal optical slice series through 1.5 μm of tissue. In this z-series, a fibroblast process can be followed from the left side of the top optical slice (left arrow in A), passing deeper within the second optical slice (B), and making close contact in the third slice (C) with a cell showing a clear myomesin banding pattern (D). A second process to the right of the top optical slice (right arrow in A) can also be followed down through subsequent slices (B and C), making close contact with another cell, in this case another fibroblast. This is evident from the next lower optical slice (D), where there is a fibroblast process coming up from deeper within the tissue in the region of the fibroblast-fibroblast contact (arrow on right-hand side). In image C′, the points of contact arrowed in C show label for Cx45, and in C″, the connexin labeling of C′ and the myomesin and vimentin labeling of C have been merged to show the exact overlay of Cx45 spots with the cell contact points. Scale bar=10 μm.

myocytes. The preferential staining of fibroblasts by LY could be related to cytoarchitectural differences (compared with myocytes) that may increase their tolerance to scrape-loading, or their ability to pass on the dye. Only cells that (1) take up the dye (via cell membrane damage) and (2) survive (heal over) can pass it on to neighboring cells (gap junctions close rapidly in dying cells). Differences in connexin expression may also play a role, because LY transfer via Cx45 is much less efficient than via Cx40.[29,30]

Dye spread was also observed in heterogeneous cell strands, consisting of fibroblasts and myocytes, shown by the presence of labeled myocytes that are interconnected only by dye-loaded fibroblasts (Figure 6). The dye-loaded myocytes are not in contact with each other (or further dye-loaded myocytes), neither in the layer illustrated, nor in higher or lower optical sections, supporting the hypothesis that dye transfer will have occurred via interconnecting fibroblasts.

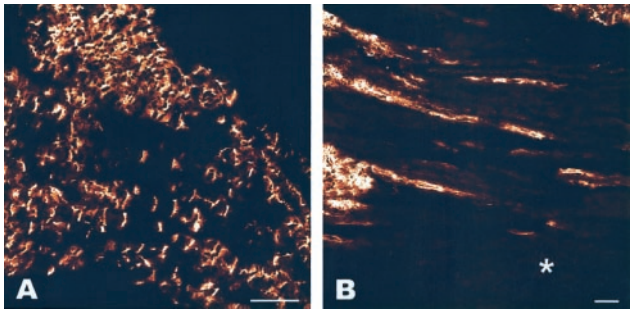

Figure 4. Cx43 in atrial muscle and SAN. A, Cx43 in atrial muscle (outside the SAN) is organized in intercalated discs. B, In the SAN periphery, Cx43 is arranged longitudinally along atrial muscle strands protruding into the node, whereas the SAN itself (asterisk in B) is negative for Cx43. Scale bars=60 μm.

Discussion

This study shows that cardiac fibroblasts express connexins in vivo and that, in rabbit SAN, they form a functionally coupled network. Results further demonstrate that SAN fibroblasts express two connexin subtypes in spatially distinct patterns: Cx40 preferentially in F-areas, and Cx45 preferentially in MF regions. The causes for this heterogeneity are unknown, but paracrine interaction with neighboring cells would form a reasonable candidate for further elucidation. Furthermore, we show that Cx45 in MF areas can be located

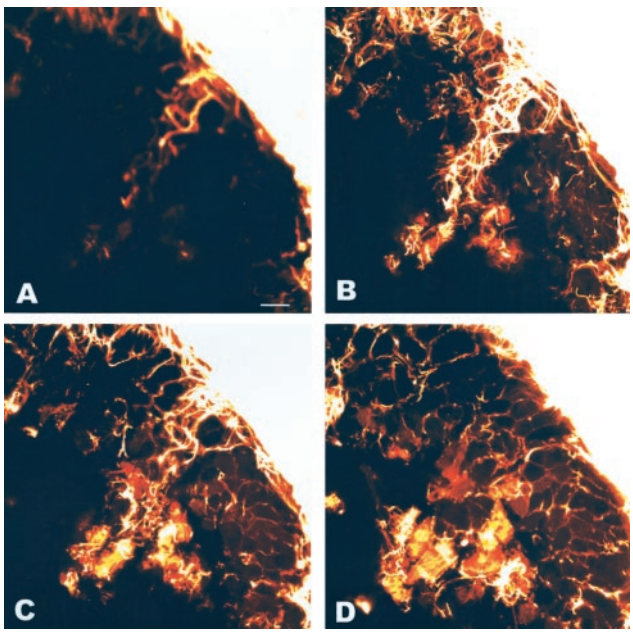

Figure 5. Confocal microscope optical slice series showing Lucifer yellow (LY) spread toward the rabbit SAN from a transmural scrape-loading site on the auricular side of the crista terminalis. The brightly labeled scrape-loading site (A through D, top right) gives rise to lateral dye spread, predominantly via cardiac fibroblasts (see strand of well-defined cell processes in A and B). These cells only contain LY (no Texas red dextrans) and will have received the dye through gap junction channels. Deeper in the tissue (lower optical slices C and D), LY-labeled myocytes are observed. We found no dye-filled myocytes above or below these, and they have presumably obtained the dye via adjacent gap junction connected fibroblasts. Individual image planes are spaced at 2.8 μm. Scale bar=20 μm.

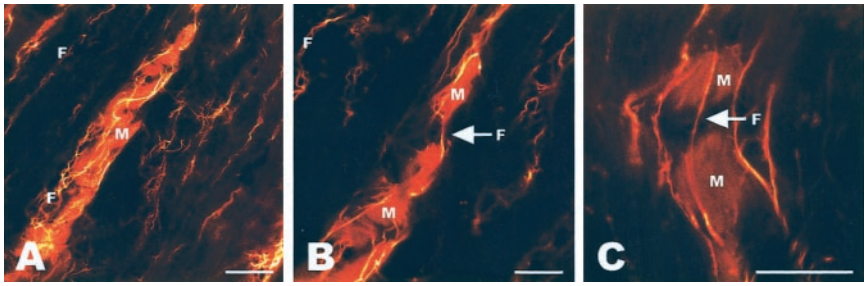

Figure 6. Lucifer yellow spread through a heterogeneous chain of fibroblasts (F; thin, brightly labeled cells) and myocytes (M; larger "orange" cells). A, Chain of dye-loaded myocytes, surrounded by densely filled fibroblasts. B, Dye-filled myocytes forming two groups interconnected only by dye-filled fibroblasts (arrow). C, Higher-magnification image of a similar juxtaposition of labeled myocytes linked by fibroblasts only (arrow). Dye spread into the myocytes must come from the adjacent dye-filled fibroblasts, as the former are not connected to other dye-loaded myocytes. Scale bars=20 μm.

between either homogeneous or heterogeneous cell pairs. Finally, dye transfer in tissue explants corroborates the existence of functional fibroblast-fibroblast and fibroblast-myocyte coupling in rabbit SAN.

Fibroblasts express Cx40 and Cx45, whose distribution appears to be affected by cell proximity. Fibroblasts in regions devoid of myocytes tend to preferentially express Cx40, whereas those that are intermingled with myocytes frequently express Cx45. This leads to a clustered patterning of connexin-subtypes in rabbit SAN. In hindsight, previous connexin labeling studies also show this "patchy" distribution of Cx40 and Cx45 (see Figures 4A and 4B in Coppen et al[11]), consistent with a cell-environment dependent connexin distribution.

In rabbit SAN, Cx45 was repeatedly located at the interface between myocyte and fibroblast membranes (214 occurrences in 33 SAN tissue samples from 8 animals; the stringent exclusion criteria suggest that, if anything, this underestimates heterogeneous coupling). The presence of Cx45 at the point of contact between fibroblasts and myocytes suggests that there may be electrical coupling between the heterogeneous cell types in vivo, as previously deduced from in situ electrophysiological evidence[5] and observed in vitro.[1,3] This is reinforced by our dye-coupling studies, which highlight a close interrelation of myocyte and fibroblast dye loading, to the extent that fibroblasts appear to contribute to dye spread between myocytes.

Electrotonic coupling of cardiac fibroblasts and myocytes could have significant consequences for cardiac electrophysiology,[4] in particular in tissue of high fibroblast content, such as the SAN or ventricular scars.[30a] Firstly, fibroblasts could act as a current sink for directly connected myocytes. Secondly, cardiac connective tissue may be involved in impulse conduction in vivo (as seen in cell culture).[2] This could either be short-range, supporting the spread of excitation between "islands" of SAN cells and in the cross-sheet direction of ventricular muscle, or long-range, "bridging" obstacles such as posttransplantation scar tissue and contributing to AV-node conduction delay. Thirdly, because fibroblasts express different connexins, they could be a target for differential regulatory effects on sites where fibroblast and myocytes intermingle (such as normal cardiac tissue, where a contribution of fibroblasts to electrical impulse conduction may be physiological), compared with sites dominated by fibroblasts (such as the aging/diseased SAN or areas of fibrosis and scarring, where connective tissue is understood to obstruct orderly conduction). Furthermore, regional differences in connective tissue density would affect regional electrical load, excitability, and/or refractoriness, whose spatial dispersion is potentially arrhythmogenic,[31–33] which might offer an alternative explanation of the repeatedly observed correlation between cardiac fibrosis and arrhythmia incidence.[34] Finally, fibroblasts are mechanosensitive[5,35] and could act as receptors, in addition to the myocytes' own ability to sense stress and strain, that contribute to cardiac mechanoelectric feedback. This may have functional advantages for cardiac autoregulation, as mechanosensors positioned outside the contractile units (ie, in cells other than myocytes) could be able to monitor the mechanical environment more reliably during cardiac contraction/relaxation.[9,36]

Thus, SAN fibroblasts in vivo express Cx40 and Cx45 in patterns that are correlated with their cellular environment. The identification of Cx45 between myocytes and nonmyocytes highlights a reasonable substrate for interaction of heterogeneous cell types in rabbit SAN. Differences to the connexin subtypes previously identified in vitro[2] may be related to differences in SAN versus ventricular connexin expression (no Cx43 in SAN) and to side-effects of cell culturing on gap junction expression. Both in vitro and in situ findings suggest, however, that one cannot rule out an active contribution of nonmyocytes to cardiac electrophysiology.

Acknowledgments

This study was conducted at the Auckland University Biomedical Imaging Research Unit, supported by the British Heart Foundation (no. 98035), the UK Medical Research Council (no. 49498), and a travel grant from the Boehringer Ingelheim Foundation. P.K. is a Royal Society Research Fellow. We are grateful to David Becker, University College London; Steven R Coppen and Nick Severs, Imperial College London; Robert G Gourdie, MUSC Charleston; and Hans M Eppenberger, ETH Zürich; for providing antibodies. We thank Bruce Smaill, University of Auckland, for his support throughout this investigation.

References

1. Rook MB, van Ginneken ACG, De Jonge B, El Aoumari A, Gros D, Jongsma HJ. Differences in gap junction channels between cardiac myocytes, fibroblasts, and heterologous pairs. *Am J Physiol*. 1992;263:C959–C977.
2. Gaudesius G, Miragoli M, Thomas SP, Rohr S. Coupling of cardiac electrical activity over extended distances by fibroblasts of cardiac origin. *Circ Res*. 2003;93:421–428.
3. Goshima K, Tonomura Y. Synchronised beating of embryonic mouse myocardial cells mediated by FL cells in monolayer culture. *Exp Cell Res*. 1969;56:387–392.
4. Kohl P. Heterogeneous cell coupling in the heart: an electrophysiological role for fibroblasts. *Circ Res*. 2003;93:381–383.

5. Kohl P, Kamkin AG, Kiseleva IS, Noble D. Mechanosensitive fibroblasts in the sino-atrial node region of rat heart: interaction with cardiomyocytes and possible role. *Exp Physiol*. 1994;79:943–956.
6. De Maziere AM, van Ginneken AC, Wilders R, Jongsma HJ, Bouman LN. Spatial and functional relationship between myocytes and fibroblasts in the rabbit sinoatrial node. *J Mol Cell Cardiol*. 1992;24:567–578.
7. Kohl P, Hunter P, Noble D. Stretch-induced changes in heart rate and rhythm: clinical observations, experiments and mathematical models. *Prog Biophys Mol Biol*. 1999;71:91–138.
8. Beny JL, Connat JL. An electron-microscopic study of smooth muscle cell dye coupling in the pig coronary arteries: role of gap junctions. *Circ Res*. 1992;70:49–55.
9. Kohl P, Noble D. Mechanosensitive connective tissue: potential influence on heart rhythm. *Cardiovasc Res*. 1996;32:62–68.
10. Anumonwo JM, Wang HZ, Trabka-Janik E, Dunham B, Veenstra RD, Delmar M, Jalife J. Gap junctional channels in adult mammalian sinus nodal cells: immunolocalization and electrophysiology. *Circ Res*. 1992; 71:229–239.
11. Coppen SR, Kodama I, Boyett MR, Dobrzynski H, Takagishi Y, Honjo H, Yeh HI, Severs NJ. Connexin45, a major connexin of the rabbit sinoatrial node, is co-expressed with connexin43 in a restricted zone at the nodal-crista terminalis border. *J Histochem Cytochem*. 1999;47:907–918.
12. Boyett MR, Honjo H, Kodama I. The sinoatrial node, a heterogeneous pacemaker structure. *Cardiovasc Res*. 2000;47:658–687.
13. Verheule S, van Kempen MJA, Postma S, Rook MB, Jongsma HJ. Gap junctions in rabbit sinoatrial node. *Am J Physiol*. 2001;280: H2103–H2115.
14. Yeh HI, Rothery S, Dupont E, Coppen SR, Severs NJ. Individual gap junction plaques contain multiple connexins in arterial endothelium. *Circ Res*. 1998;83:1248–1263.
15. Coppen SR, Dupont E, Rothery S, Severs NJ. Connexin45 expression is preferentially associated with the ventricular conduction system in mouse and rat heart. *Circ Res*. 1998;82:232–243.
16. Wright CS, Becker DL, Lin JS, Warner AE, Hardy K. Stage-specific and differential expression of gap junctions in the mouse ovary: connexin-specific roles in follicular regulation. *Reproduction*. 2001;121:77–88.
17. Grove BK, Kurer V, Lehner C, Doetschman TC, Perriard JC, Eppenberger HM. A new 185,000-dalton skeletal muscle protein detected by monoclonal antibodies. *J Cell Biol*. 1984;98:518–524.
18. Osborn M, Debus E, Weber K. Monoclonal antibodies specific for vimentin. *Eur J Cell Biol*. 1984;34:137–143.
19. Bohn W, Wiegers W, Beuttenmuller M, Traub P. Species-specific recognition patterns of monoclonal antibodies directed against vimentin. *Exp Cell Res*. 1992;201:1–7.
20. Warner AE, Bate CM. Techniques for dye injection and labelling. In: Standen NB, Gray PTA, Whitaker MJ, eds. *Microelectrode Techniques: The Plymouth Workshop Handbook*. Cambridge, UK: Company of Biologists Ltd; 1987:187–198.
21. Becker DL, Green CR. Gap junction mediated interactions between cells. In: Fleming TP, ed. *Cell-Cell Interaction: A Practical Approach*. 2nd ed. Oxford, UK: Oxford University Press; 2002:47–70.
22. Meda P. Assaying the molecular permeability of connexin channels. In: Bruzzone R, Giaume C, eds. *Connexin Methods and Protocols*. Humana Press; 2001:201–224.
23. Becker DL, Dekkers J, Navarrete R, Green CR, Cook JE. Enhancing the laser scanning confocal microscopic visualization of Lucifer yellow filled cells in whole-mounted tissue. *Scanning Microsc*. 1991;5:619–624.
24. ten Velde I, de Jonge B, Verheijck EE, van Kempen MJ, Analbers L, Gros D, Jongsma HJ. Spatial distribution of connexin43, the major cardiac gap junction protein, visualizes the cellular network for impulse propagation from sinoatrial node to atrium. *Circ Res*. 1995;76:802–811.
25. Peters NS, Severs NJ, Rothery SM, Lincoln C, Yacoub MH, Green CR. Spatiotemporal relation between gap junctions and fascia adherens junctions during postnatal development of human ventricular myocardium. *Circulation*. 1994;90:1103–1106.
26. Smith JH, Green CR, Peters NS, Rothery S, Severs NJ. Altered patterns of gap junction distribution in ischemic heart disease: an immunohistochemical study of human myocardium using laser scanning confocal microscopy. *Am J Pathol*. 1991;139:801–821.
27. Davis LM, Rodefeld ME, Green K, Beyer EC, Saffitz JE. Gap junction protein phenotypes of the human heart and conduction system. *J Cardiovasc Electrophysiol*. 1995;6:813–822.
28. Kwong KF, Schuessler RB, Green KG, Laing JG, Beyer EC, Boineau JP, Saffitz JE. Differential expression of gap junction proteins in the canine sinus node. *Circ Res*. 1998;82:604–612.
29. Martinez AD, Hayrapetyan V, Moreno AP, Beyer EC. Connexin43 and connexin45 form heteromeric gap junction channels in which individual components determine permeability and regulation. *Circ Res*. 2002;90: 1100–1107.
30. van Rijen HV, van Veen TA, Hermans MM, Jongsma HJ. Human connexin40 gap junction channels are modulated by cAMP. *Cardiovasc Res*. 2000;45:941–951.

30a. Camelliti P, Devlin GP, Matthews KG, Kohl P, Green CR. Spatially and temporally distinct expression of fibroblast connexins after sheep ventricular infarction. *Cardiovasc Res*. In press.

31. Stilli D, Aimi B, Sgoifo A, Ciarlini P, Regoliosi G, Lagrasta C, Olivetti G, Musso E. Dependence of temporal variability of ventricular recovery on myocardial fibrosis: role of mechanoelectric feedback? *Cardiovasc Res*. 1998;37:58–65.
32. Kamkin A, Kiseleva I, Wagner KD, Leiterer KP, Theres H, Scholz H, Gunther J, Lab MJ. Mechano-electric feedback in right atrium after left ventricular infarction in rats. *J Mol Cell Cardiol*. 2000;32:465–477.
33. Kamkin A, Kiseleva I, Wagner KD, Pylaev A, Leiterer KP, Theres H, Scholz H, Gunther J, Isenberg G. A possible role for atrial fibroblasts in postinfarction bradycardia. *Am J Physiol*. 2002;282:H842–H849.
34. Vasquez C, Moreno AP, Berbari EJ. A model of the biophysical basis of fractionated electrograms and microreentry based on gap junction coupling between myocytes and fibroblasts. *Pacing Clin Electrophysiol*. 2003;26:977.
35. Stockbridge LL, French AS. Stretch-activated cation channels in human fibroblasts. *Biophys J*. 1988;54:187–190.
36. Kohl P, Varghese A, Dekanski J, Noble D, Winslow RL. Computational study of the impact of cardiac mechanosensitive fibroblasts on heart rhythm. *Exp Clin Cardiol*. 1996;1:80–86.